Mg^{2+} mediates interaction between the voltage sensor and cytosolic domain to activate BK channels

Huanghe Yang[†], Lei Hu[†], Jingyi Shi[†], Kelli Delaloye[†], Frank T. Horrigan[‡], and Jianmin Cui[†§]

[†]Department of Biomedical Engineering and Cardiac Bioelectricity and Arrhythmia Center, Washington University, St. Louis, MO 63130; and [‡]Department of Physiology, University of Pennsylvania, Philadelphia, PA 19104-6085

Edited by Ramón Latorre, Centro de Estudios Científicos, Valdivia, Chile, and approved September 25, 2007 (received for review June 22, 2007)

The voltage-sensor domain (VSD) of voltage-dependent ion channels and enzymes is critical for cellular responses to membrane potential. The VSD can also be regulated by interaction with intracellular proteins and ligands, but how this occurs is poorly understood. Here, we show that the VSD of the BK-type K^+ channel is regulated by a state-dependent interaction with its own tethered cytosolic domain that depends on both intracellular Mg^{2+} and the open state of the channel pore. Mg^{2+} bound to the cytosolic RCK1 domain enhances VSD activation by electrostatic interaction with Arg-213 in transmembrane segment S4. Our results demonstrate that a cytosolic domain can come close enough to the VSD to regulate its activity electrostatically, thereby elucidating a mechanism of Mg^{2+}-dependent activation in BK channels and suggesting a general pathway by which intracellular factors can modulate the function of voltage-dependent proteins.

electrostatic interaction | interdomain interaction | magnesium | Ca^{2+}-activated K^+ channel | metal ion regulation

Voltage-dependent ion channels are modular proteins (1) containing four voltage-sensor domains (VSDs) that control the opening and closing of a central pore domain. Each VSD contains charged residues in transmembrane segments that sense changes in membrane potential. VSDs are important for controlling not only ion channel pores but also enzymatic activity (2) and can serve as stand-alone proton channels in the absence of a separate pore domain (3, 4). Because VSDs impact multiple aspects of cellular function, it is important to understand how VSD function is regulated. Many intracellular factors such as ligand binding, post-translational modification, and the presence of cytosolic domains, accessory proteins, or subunits can alter the function of voltage-dependent ion channels (5). In some cases such modulation is thought to involve the voltage sensor (6–10). However, the mechanisms by which intracellular factors and VSDs interact are poorly understood. BK channels are activated by membrane depolarization, intracellular Ca^{2+}, and Mg^{2+} (11) and are essential for modulating muscle contraction and neuronal activities such as synaptic transmission and hearing (12, 13). Like other voltage-dependent K^+ (Kv) channels, BK channels possess a VSD where the S4 segment contains multiple Arg residues (14, 15). However, in BK channels, only one of these, R213, contributes to voltage sensing (15–18). Interestingly, neutralizing R213 by mutation (R213Q) not only alters voltage-dependent activation but also abolishes Mg^{2+}-dependent activation of BK channels, revealing that the VSD contributes to Mg^{2+} sensitivity, although the mechanism is unknown (18). Here, we investigate the mechanism of Mg^{2+} action to determine whether and how the VSD interacts with Mg^{2+} ions that are bound to the BK channel's COOH-terminal cytosolic domain.

Results

Mg^{2+} May Activate the VSD by Electrostatic Interaction. Physiological concentrations of Mg^{2+} in the low millimolar range activate BK channels, independent of the effects of micromolar Ca^{2+}, by binding to a site that includes residues E374 and E399 (19–21). The putative Mg^{2+} binding site is located in a cytosolic domain that is homologous to the RCK1 domain of MthK and *Escherichia coli* K^+ channels (19, 22–25). Fig. 1*a* shows the structure of the cytosolic domain of MthK, in which the residues at positions corresponding to E374 and E399 of the mSlo1 BK channel (E138, N158) have been changed to Glu and colored red. The Mg^{2+} binding site is apparently exposed on the surface of the RCK1 domain, facing the membrane. The distance between the Mg^{2+} binding site and the central axis of the MthK channel pore (≈31 Å) roughly coincides with that between the C terminus of S4 and the central axis of the Kv1.2 channel (Fig. 1*a*, yellow circle), suggesting that the Mg^{2+} site and VSD of the BK channel may lie close together. However, the detailed structure of the BK channel is unknown. Moreover, the BK channel is a complex allosteric protein whose cytosolic domain is thought to undergo conformational changes associated with ligand binding and channel opening (11). Therefore, it is not clear whether Mg^{2+} and the VSD interact directly or indirectly, through what physical mechanism, or in which conformational state(s). One possibility, depicted in Fig. 1*b*, is that the binding of the Mg^{2+} may alter the local electric field that is sensed by charged residues in the VSD, thereby activating the channel. This hypothesis is consistent with the fact that Mg^{2+} shifts the voltage dependence of channel opening to more negative voltages and that the neutralization of R213 abolishes Mg^{2+} sensitivity (18). Another line of evidence supporting this hypothesis is that Mg^{2+}-dependent activation is sensitive to the ionic strength of intracellular solution. In our normal intracellular solution with intracellular K^+ concentration ($[K^+]_i$) = 142 mM (see *Methods*), 10 mM Mg^{2+} activates the channel by shifting the voltage dependence of conductance (*G-V* relationship) to more negative voltages $\Delta V_{1/2} = -60 \pm 3.8$ mV, where $V_{1/2}$ is the voltage at half-maximum conductance (Fig. 1 *c* and *d*). The amount of *G-V* shift caused by 10 mM Mg^{2+} increases in lower $[K^+]_i$ and decreases in higher $[K^+]_i$ (Fig. 1*e*), as expected if Mg^{2+} activates the channel by an electrostatic interaction. To the contrary, ionic strength does not significantly affect Ca^{2+}-dependent activation (Fig. 1*e*), suggesting that Ca^{2+} does not activate the channel by an electrostatic interaction and the changes in ionic strength do not affect Ca^{2+} binding. Similarly, the strong response of Mg^{2+}-dependent activation to ionic strength may not reflect changes in Mg^{2+} binding.

A Positive Charge on Residue 397 Produces Effects Similar to Mg^{2+}. To further test the idea that an electrostatic interaction underlies Mg^{2+} action, we compared the effects on BK channel gating of Mg^{2+} with those of adding charges to position 397 (Q397; Fig. 1 *a* and *b*). Q397

Author contributions: H.Y. and L.H. contributed equally to this work; H.Y., L.H., and J.C. designed research; H.Y., L.H., J.S., and K.D. performed research; F.T.H. contributed new reagents/analytic tools; H.Y. and L.H. analyzed data; and H.Y., F.T.H., and J.C. wrote the paper.

The authors declare no conflict of interest.

This article is a PNAS Direct Submission.

Abbreviations: VSD, voltage-sensor domain; Kv, voltage-dependent K^+; $V_{1/2}$, voltage at half-maximum conductance; V_{hc}, voltage for half of the gating charge movements at the closed conformation of the channel; I_g, gating current; I_{gON}, on I_g; I_{gOFF}, off I_g; I_K, K^+ ionic current; $[Mg^{2+}]_i$, intracellular Mg^{2+} concentration; $[K^+]_i$, intracellular K^+ concentration; P_o, open probability; $[Ca^{2+}]_i$, intracellular Ca^{2+} concentration.

§To whom correspondence should be addressed. E-mail: jcui@biomed.wustl.edu.

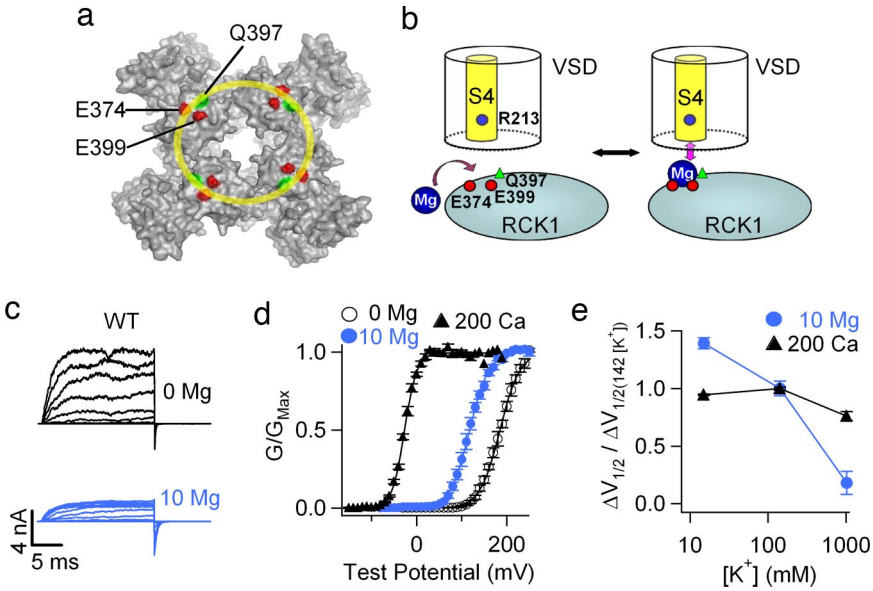

Fig. 1. Mg^{2+} may activate the BK channel by an electrostatic interaction. (*a*) The crystal structure of the cytosolic domain of the MthK channel (Protein Data Bank ID code 1LNQ, top view from the cytoplasmic membrane), in which E138 corresponds to E374 of the mSlo1 channel, while G156 and N158 were mutated to the corresponding Q397 and E399. The yellow circle indicates the distance from the β-carbon of R303 in S4 to the central axis in the Kv1.2 crystal structure (Protein Data Bank ID code 2A79) (1). R303 of Kv1.2 corresponds to R213 in mSlo1. (*b*) Mg^{2+} binds to the site in the cytosolic RCK1 domain and interacts with R213 to affect the voltage sensor movement. (*c*) Current traces of WT mSlo1 channels in 0 and 10 mM $[Mg^{2+}]_i$. Testing potentials were −30 to 230 mV with 20-mV increments. Both holding and repolarizing potentials were −80 mV. (*d*) Mean *G-V* relations of WT channels in 0 $[Mg^{2+}]_i$, 10 mM $[Mg^{2+}]_i$, and 200 μM $[Ca^{2+}]_i$. (*e*) Effects of ionic strength on Mg^{2+} and Ca^{2+} sensing of WT mSlo1. $\Delta V_{1/2}$ equals the $V_{1/2}$ change from 0 to 10 mM $[Mg^{2+}]_i$ or from 0 to 200 μM $[Ca^{2+}]_i$ in specific $[K^+]_i$. $\Delta V_{1/2(142[K+])}$ is the $V_{1/2}$ change in 142 mM$[K^+]_i$ and equals −60.7 ± 3.8 mV for Mg^{2+} sensing and −214.3 ± 2.8 mV for Ca^{2+} sensing, respectively. $V_{1/2}$ is the voltage where the *G-V* relation is half maximum and obtained by fitting the *G-V* relation to the Boltzmann function (see *Methods*).

lies close to the Mg^{2+}-binding site, based on the MthK structure, and it is only one residue away from E399 in the primary sequence. Our previous results suggest that adding charges to this position by mutation or chemical modification does not abolish Mg^{2+}-dependent activation but affects Mg^{2+} sensitivity through electrostatic interaction with the bound Mg^{2+} (21). Thus, the electric field of the charge at position 397 overlaps that of bound Mg^{2+}. Therefore, if our hypothesis is correct, a positive charge at position 397 should have effects on channel activation that are qualitatively similar to those of Mg^{2+}, as if a cation was constitutively bound near the Mg^{2+} site.

Consistent with the above prediction, mutations of Q397 to positively charged amino acids (Q397K, Q397R) activate the channel by shifting the *G-V* relation to more negative voltages in the absence of intracellular Mg^{2+} (Fig. 2 *a* and *b*). Also consistent with an electrostatic interaction, mutations of Q397 to negatively charged amino acids (Q397E, Q397D) shift the *G-V* relation to more positive voltages, whereas Q397C has insignificant effects on the *G-V* relation ($P > 0.05$). Similar to Mg^{2+}-dependent activation, the *G-V* shift caused by mutation Q397K is also affected by ionic strength (Fig. 2*c*). The fractional changes of $\Delta V_{1/2}$ caused by Mg^{2+} and the mutation superimpose at low $[K^+]_i$ and only differ at high $[K^+]_i$. Because the mutation adds a charge permanently to the channel, this result further suggests that changing ionic strength alters Mg^{2+}-dependent activation primarily by affecting an electrostatic interaction, with only a small effect on Mg^{2+} binding. BK channels traverse multiple states during activation (11). Interestingly, the change in electric field produced by Mg^{2+} binding is not felt uniformly by all these transitions. Unlike the *G-V* relation, the voltage dependence of activation kinetics (τ-*V* relation) is not shifted by increasing intracellular Mg^{2+} concentration ($[Mg^{2+}]_i$) from 0 to 10 mM (27–29).[¶] Similarly, the mutations Q397R and Q397K do not shift the τ-*V* relation (Fig. 2*d*), further supporting that positive charges at position 397 affect the same set of gating transitions as Mg^{2+}.

The effects of adding a positive charge to position 397 by chemical modification also mimic qualitatively the effects of Mg^{2+} binding on the *G-V* relation (Fig. 2 *e* and *f*). In this experiment, the Q397C mutant was treated with the Cys-modifying reagent MTSET(+) at the intracellular side during patch-clamp recordings. Because MTSET(+) is known to alter the voltage dependence of WT BK channels by modifying C430 (30), the channels in our study contained another mutation C430A to eliminate this background effect of MTSET(+). Modification of Q397C by MTSET(+) shifted the *G-V* relation to more negative voltages in the absence of Mg^{2+}, indicating that the covalent addition of a positive charge to Q397C activates the channel. The results in Fig. 2 suggest that the gating of the BK channel is affected primarily by alterations in charge near the Mg^{2+}-binding site. Nevertheless, it is worth noting that there are differences in the *G-V* shift produced by mutation and chemical modification of position 397 and Mg^{2+} binding, which may reflect differences in the number, orientation, and environment of charges as well as their distance relative to the VSD.

State-Dependent Interaction Between Mg^{2+} and VSD. The movement of the voltage sensor in response to a change in voltage generates a transient gating current (I_g). If Mg^{2+} activates the channel through electrostatic interactions with the VSD, it should alter I_g. BK channel voltage sensors can move between the resting and activated state and generate gating current no matter whether channels are closed or open (16, 31) (Fig. 3). However, voltage-sensor activation occurs at less depolarized voltages in the open conformation, thereby promoting voltage-dependent opening (31). The results in Fig. 3 show that, consistent with our hypothesis, Mg^{2+} enhances voltage-sensor activation, but interestingly, Mg^{2+} acts primarily when channels are open and has little effect when channels are closed.

On I_g (I_{gON}) elicited by a depolarizing voltage pulse is associated

[¶]Horrigan FT (2005) *Biophys J* 88:100A (abstr).

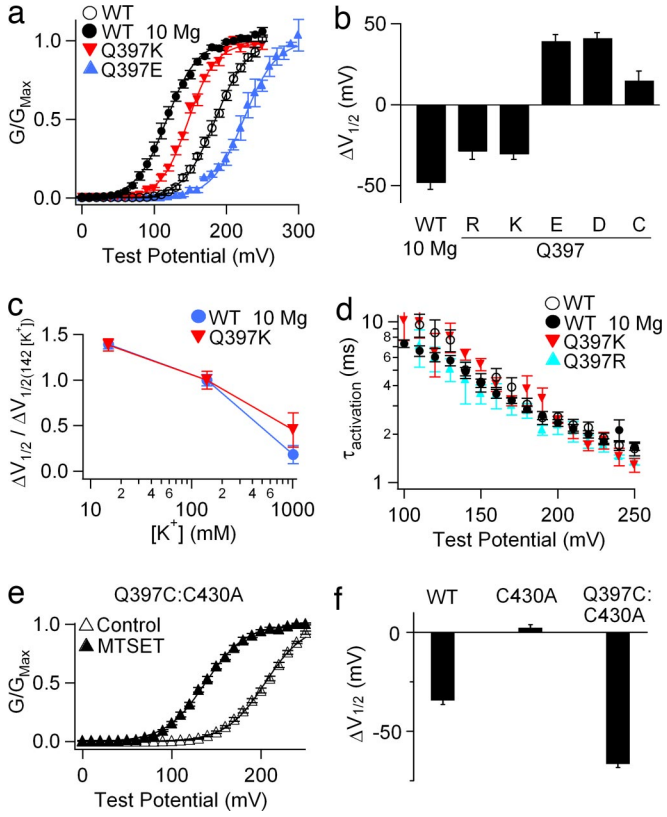

Fig. 2. Mg^{2+} and a positive charge at residue 397 have similar effects on the voltage dependence of I_K. (*a*) Mean *G-V* relations of WT, Q397K, and Q397E in 0 $[Mg^{2+}]_i$ compared with that of WT in 10 mM $[Mg^{2+}]_i$. (*b*) Shifts of the *G-V* relation caused by 10 mM $[Mg^{2+}]_i$ for the WT mSlo1 and by Q397 mutations in 0 $[Mg^{2+}]_i$. Here and in Fig. 4*a* the *G-V* shift of WT channel from 0 to 10 mM $[Mg^{2+}]_i$ is subtracted by −12.2 mV because of Mg^{2+} binding to another low-affinity Mg^{2+} site (28). There is no statistically significant difference between the $V_{1/2}$s of WT and Q397C (Student's *t* test, $P > 0.05$). (*c*) Effects of ionic strength on Mg^{2+} sensing of WT channels (the same data as in Fig. 1*d*) and the *G-V* shift of Q397K relative to WT channels in 0 $[Mg^{2+}]_i$. $\Delta V_{1/2(142[K+])}$ equals −30.8 ± 3.0 mV for Q397K-induced shift. (*d*) Mean activation time constants as a function of voltage. (*e*) Mean *G-V* relations of Q397C:C430A mutant channels in 0 $[Mg^{2+}]_i$ before and after MTSET(+) treatment. (*f*) *G-V* shifts of WT, C430A, and Q397C:C430A mutant channels induced by MTSET(+) treatment in 0 $[Mg^{2+}]_i$.

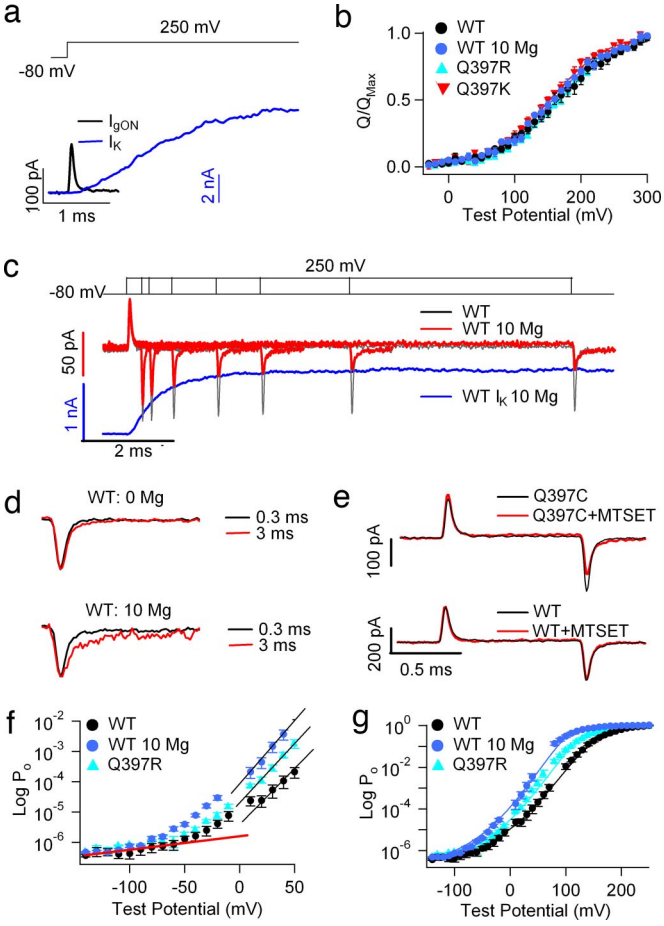

Fig. 3. Mg^{2+} and a positive charge at residue 397 have similar effects on gating current and limiting slope measurements. (*a*) I_{gON} (black) and I_K (blue) traces for mSlo1 channels. (*b*) Q_C-*V* relations for WT, Q397R, and Q397K channels. Solid lines are fits to the Boltzmann relation. (*c*) Gating current traces for WT channels elicited by voltage pulses to 250 mV with durations of 0.3, 0.5, 1, 2, 5, and 10 ms. The peaks of I_{gOFF} at 10 mM $[Mg^{2+}]_i$ (red) are aligned with an I_K trace (blue) measured at the same voltage and $[Mg^{2+}]_i$. The time constant of I_K is 0.92 ms. (*d*) Superposition of I_{gOFF} currents after 0.3 (black) and 3 ms (red) pulses to 250 mV for WT channels in 0 and 10 mM $[Mg^{2+}]_i$, respectively. The amplitudes of I_{gOFF} after 3-ms pulse were normalized to the corresponding I_{gOFF} amplitude after 0.3-ms pulse. (*e*) I_g traces for WT channel and Q397C mutation before (black) and after (red) 200 μM MTSET(+) treatment. (*f* and *g*) P_o-*V* relations. Straight lines indicate the slope of the curves at different voltage ranges (*f*) or fits to the HCA model (*g*). The fitting parameters are: $L_0 = 1.5e\text{-}6$, $Z_J = 0.57$, $Z_L = 0.3$; for WT channel in 0 $[Mg^{2+}]_i$: $V_{hc} = 167$ mV, $V_{ho} = 17$ mV; for WT channel in 10 mM $[Mg^{2+}]_i$: $V_{hc} = 157$ mV, $V_{ho} = -33$ mV; for Q397R in 0 $[Mg^{2+}]_i$: $V_{hc} = 167$ mV, $V_{ho} = -7$ mV. All measurements were made in 0 $[Mg^{2+}]_i$ unless indicated otherwise.

with movement of the voltage sensor from the resting to the activated state, and in BK channels it is very rapid compared with the opening of the pore and rise of K^+ current (Fig. 3*a*). Thus the movement of the voltage sensor is essentially complete before channels open, and I_{gON} reflects voltage sensor movement when channels are closed. The amplitude of I_{gON} is slightly larger in 10 mM than in 0 $[Mg^{2+}]_i$ (≈10% increase at +250 mV; data not shown), whereas the time course of I_{gON} is not altered (Fig. 3*c*). The relationship between gating charge movement and membrane voltage when channels are closed (Q_C-*V* relation), determined by integrating the area under the I_{gON} traces at various voltages, exhibits no significant change between 0 and 10 mM $[Mg^{2+}]_i$ (Fig. 3*b*) (≈10-mV difference in the voltage at the half-maximum of the Q_C-*V* relation, V_{hc}). These results indicate that Mg^{2+} does not affect the closed channel significantly, which may also explain why K^+ ionic current (I_K) activation kinetics are insensitive to Mg^{2+} (Fig. 2*d*).

On the other hand, off I_gs (I_{gOFF}), which reflect the return of the voltage sensor from the activated to the resting state, are decreased in amplitude and slowed by 10 mM $[Mg^{2+}]_i$ (Fig. 3 *c* and *d*). Under our experimental conditions (see *Methods*) K^+ currents through the pore are blocked but channels are still open in response to depolarization (31). Therefore, a fraction of channels are open at the end of a voltage pulse when I_{gOFF} is recorded. To examine whether the change of I_{gOFF} is related to the fraction of open channels, we measured I_{gOFF} after pulses of various duration (Fig. 3*c*). After a 0.30-ms voltage pulse, few channels are open and I_{gOFF} is similar in the presence or absence of Mg^{2+}. However, as pulse duration increases I_{gOFF} amplitude is greatly reduced in 10 mM $[Mg^{2+}]_i$ (red traces, Fig. 3*c*), indicating that Mg^{2+} affects voltage sensor movement more significantly when channels are open. Previous studies indicate that voltage-sensor deactivation is slowed when channels are open even in the absence of Mg^{2+} (31, 32) (Fig. 3*d*). In our experiment at +250 mV, channels should be almost maximally activated in the presence or absence of Mg^{2+} (Figs. 1*d* and 3*b*).

Therefore, the greater effect on I_{gOFF} in 10 mM $[Mg^{2+}]_i$ (Fig. 3*d*) does not merely reflect a change in open probability but rather implies that deactivation of voltage sensors in open channels is slowed by Mg^{2+}.

The charge-voltage relation for open BK channels (Q_O-V) is difficult to measure directly from gating currents because, in contrast to the case of voltage-sensor activation and channel opening (Fig. 3*a*), the time course of voltage-sensor deactivation is not much faster than channel closing (31). However, a shift in the Q_O-V relation to more negative voltages caused by 10 mM $[Mg^{2+}]_i$ is evident from the voltage dependence of open probability (P_o) at negative voltages (Fig. 3*f*). BK channels can open even when voltage sensors are in the resting state; thus P_o can be measured at voltages more negative than the range of voltage-sensor activation (33). Such openings have weak voltage dependence as indicated by the red line in Fig. 3*f*. At more positive voltages the $Log(P_o)$-V relation becomes steeper (solid lines in Fig. 3*f*) because of voltage-sensor activation, and this inflection in slope provides an indication of the position of the Q_O-V relation along the voltage axis (32). Clearly, Mg^{2+} does not affect channel opening when the voltage sensor is in the resting state because the $Log(P_o)$-V relations in 0 and 10 mM $[Mg^{2+}]_i$ superimpose at the most negative voltages. Mg^{2+} increases P_o only at potentials where voltage sensors can activate and shifts the inflection point in the $Log(P_o)$-V relation to more negative voltages, indicating that Mg^{2+} enhances voltage-sensor activation when the channel is open. This result is consistent with an earlier report (26). Fitting the $Log(P_o)$-V relations over a wide range of the P_o with a well established model that describes the voltage-dependent activation of BK channels (33) (see *Methods*) reveals that 10 mM $[Mg^{2+}]_i$ shifts the Q_o-V relation by -50 ± 2 mV (Fig. 3*g*).

Similar to Mg^{2+} binding, a positive charge at residue 397 enhances voltage-sensor activation more when channels are open. Q_C-V relations for the mutant channels Q397R and Q397K are similar to those of the WT (Fig. 3*b*). Modification of the Q397C channel by MTSET(+) reduces the amplitude and slows the relaxation of I_{gOFF} but leaves I_{gON} unchanged (Fig. 3*e*). The mutation Q397R, like Mg^{2+}, has no effect on P_o at very negative voltages, but shifts voltage-sensor activation for open channels to more negative voltages by -24 ± 2 mV (Fig. 3 *f* and *g*), similar to the shift in the *G-V* relation by Q397R (Fig. 2*c*). Because the Q397R channel is still sensitive to Mg^{2+} (21), the charges of the Arg side chain and the bound Mg^{2+} must be located at different positions. Given this difference, the similar effects on voltage-sensor activation and channel opening produced by the spatially separated Arg at 397 and bound Mg^{2+} suggest that the interaction between cytosolic and VSDs is mediated by long-range electrostatic interactions.

R213 in Transmembrane Segment S4 Senses Mg^{2+}. Which residues in the VSD sense the changes in the electric field as a result of Mg^{2+} binding and are responsible for the functional changes in channel gating? Analysis of the primary sequence of BK channels indicates that 12 charged residues in the VSD (S1–S4 and the S4–S5 linker) may be exposed to cytosol. We mutated each of these residues individually to alter their charge and examined the effects of these mutations on the shift of the *G-V* relation in response to 10 mM Mg^{2+} (Fig. 4*a*). Of all of these mutations, only R213C completely abolishes Mg^{2+} sensitivity (Fig. 4 *a* and *b*), consistent with the previous finding that R213Q abolishes Mg^{2+} sensitivity (18). Residue 213 is located in the C-terminal half of S4, is accessible to intracellular Cys-modifying reagents when the voltage sensor is in the resting state (18), and contributes to gating charge (14, 15). Thus, this residue is a sensor of both membrane voltage and Mg^{2+} binding. Fig. 4*b* shows that when R213 is mutated to Cys the substitution of a positively charged residue at position 397 (the double mutation R213C:Q397R) no longer shifts the *G-V* relation to negative voltages, supporting that R213 is the main sensor of

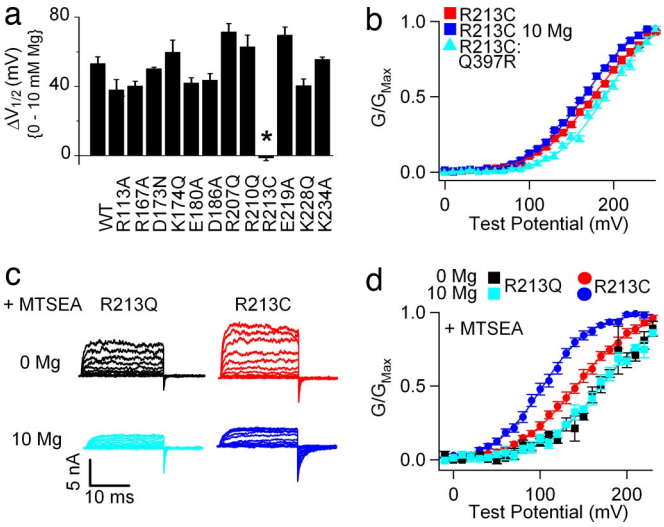

Fig. 4. Intracellular Mg^{2+} moves the voltage sensor by electrostatic interaction with R213. (*a*) Shifts of the *G-V* relation caused by an increase of $[Mg^{2+}]_i$ from 0 to 10 mM for WT and mutant channels. The *G-V* relations were measured in 0 $[Ca^{2+}]_i$ except for that of R213C (*, measured in 100 μM $[Ca^{2+}]_i$). (*b*) Mean *G-V* relations for R213C and R213C:Q397R. (*c* and *d*) Current traces (*c*) and mean *G-V* relations (*d*) for R213Q and R213C after MTSEA(+) treatment. Testing potentials were -80 to 200 mV with 20-mV increments. Both holding and repolarizing potentials were -80 mV. In *b–d* all measurements were made in 100 μM $[Ca^{2+}]_i$ and 0 $[Mg^{2+}]_i$ unless indicated otherwise.

charges around the Mg^{2+}-binding site. Finally, if Mg^{2+} activates the channel by an electrostatic interaction with the charge of R213, adding a positive charge back to position 213 should rescue some of the Mg^{2+} sensitivity that is lost because of the R213C mutation. As expected, modification of R213C channels, but not R213Q, by MTSEA(+) restores Mg^{2+} sensitivity such that the deactivation of the channel is slowed down and the *G-V* relation is shifted to more negative voltages by 10 mM Mg^{2+} (Fig. 4 *c* and *d*). The results in Fig. 4 indicate that a positive charge at residue 213 is sufficient and necessary for the VSD to sense Mg^{2+} binding and bears the primary responsibility for Mg^{2+}-dependent activation.

Discussion

Our results demonstrate that in BK channels the VSD senses not only membrane voltage but also intracellular Mg^{2+} to control channel activation (Fig. 1*b*). Mg^{2+} binding in the cytosolic domain alters the electric field at R213 in S4 to promote the occupation of the activated state by the voltage sensor, thereby favoring the open state of the channel. This mechanism is based on three lines of evidence: (*i*) Mg^{2+}-dependent activation strongly depends on intracellular ionic strength, (*ii*) positive charges at residue 397, close to the Mg^{2+}-binding site, alter channel gating similarly to Mg^{2+} in all major aspects, whereas negative charges at this site inhibit activation, and (*iii*) a positive charge at residue 213 in S4 is necessary and sufficient to sustain Mg^{2+} sensitivity. Although intracellular ionic strength influences Mg^{2+}-dependent activation, it has only a small effect on Ca^{2+}-dependent activation (Fig. 1*e*). Similarly, charges at residues 397 and 213 have little effect on Ca^{2+} sensitivity (ref. 17 and data not shown). Considering that the Mg^{2+}-binding site is located in the N-terminal half of the RCK1 domain, which is also important for Ca^{2+}-dependent activation (34), these results suggest that Mg^{2+} or the charges at residue 397 do not cause a global change in channel structure. Rather, they are involved in a local interaction specific for Mg^{2+}-dependent activation. On the other hand, the charges at residue 397 were able to reproduce the effects of Mg^{2+} on channel gating regardless if they were introduced via mutation or cysteine modification, and differences in side-chain

size, orientation, or charge distribution only result in minor quantitative variations of the effects. These results are compatible with a long-range electrostatic interaction.

During voltage-dependent activation, S4 moves in response to voltage changes to open the channel. Our results indicate that R213 in BK channel S4 can be sufficiently close to its tethered cytosolic domain to interact electrostatically with bound Mg^{2+} and charge at residue 397. Because the energy of the electrostatic interaction is manifested as a shift in the Q_o-V relation we can estimate the average distance between the charges of R213 and R397 as follows. Because voltage sensors in each of the four BK channel α-subunits are thought to activate independently via a two-state process (31, 32), the energy to shift the Q_O-V is:

$$\Delta G[Q_O] = \Delta V_{1/2} * z_g, \quad [1]$$

where z_g is the gating charge per voltage sensor ($z_g = 0.58e$) (15) and $\Delta V_{1/2} = -24$ mV (Fig. 3 *f* and *g*). The energetic effect on voltage-sensor activation produced by electrostatic interaction of Q397R with R213 is:

$$\Delta G[R213] = (\psi_R - \psi_A) * z_{R213}, \quad [2]$$

where ψ_R and ψ_A are the electrostatic potentials imposed by 397R on R213 in the resting and activated state, respectively, and z_{R213} is the charge of R213 ($z_{R213} = e$). Because ψ falls off quickly with distance and in the activated state R213 is likely to be buried in the protein because it is a gating charge (15), we can assume $\psi_A \ll \psi_R$. Thus, combining Eqs. **1** and **2** to solve for $\Delta G[Q_O] = \Delta G[R213]$ yields:

$$\psi_R = 0.58 * \Delta V_{1/2}. \quad [3]$$

This electrostatic potential between the charges of R213 and R397 ($\psi_R = 13.9$ mV) implies that the average distance between them in the resting state is 9.1 Å (see *Methods* for calculation). This calculation may overestimate the distance if R213 also interacts with 397R when the voltage sensor is in the activated state. Such a short distance between the membrane-spanning and the cytosolic domains in BK channels is consistent with the structure of BK channels, in which a short peptide linker of only 17 aa connects S6 to the cytosolic domain (35). Thus it is reasonable to expect that close interaction between the membrane spanning and the cytosolic domains can occur.

We find that the effect of Mg^{2+} is state-dependent, enhancing voltage-sensor activation primarily when the channel is open. Although Mg^{2+} has been proposed to bind with lower affinity to closed than open channels (36), state-dependent binding cannot account for the lack of effect of Mg^{2+} on Q_C-V. First, 10 mM $[Mg^{2+}]_i$ is higher than the estimated dissociation constant of the closed channel (36) so that more than half of the Mg^{2+}-binding sites should be occupied when channels are closed. Second, the permanent addition of positive charge at residue 397 near the Mg^{2+}-binding site also has no effect on Q_C-V (Fig. 2*b*). Taken together, these results indicate that the interaction between the bound Mg^{2+} and the VSD is state-dependent, presumably involving a conformational change in the cytosolic domain and/or VSD upon channel opening that exposes R213 to the electric field of the bound Mg^{2+}. One possibility is that the distance between R213 and the bound Mg^{2+} is enlarged in the closed state because of the relative movements between S4 and the cytosolic domain. The crystal structures of MthK channels suggest that the cytosolic gating ring may expand 8 Å at the outer rim in parallel to the membrane from the closed to the open conformation (37). On the other hand, in BK (15) and Shaker (38) K^+ channels rearrangements of the VSD have been suggested to occur upon channel opening. Similar changes in BK channels may change the distance between R213 and the bound Mg^{2+}. Another possibility is that the conformational rearrangements in the VSD and the cytosolic domain during channel opening may change the orientation of R213 or the bound Mg^{2+} such that the side chain of R213 is only exposed to the electric field of the bound Mg^{2+} in the open state. The detailed mechanism of the state dependence of Mg^{2+} modulation is not known at this time. Nevertheless, it is clear that VSD activity is regulated not only by Mg^{2+} bound to the cytosolic domain but also by feedback from the activation gate in the pore domain.

Aside from elucidating the mechanism of Mg^{2+}-dependent activation in BK channels, our results also demonstrate that a tethered cytosolic protein domain can come close enough to the VSD to regulate its activity through electrostatic interaction. This interaction sets precedence that various cytosolic domains, accessory subunits, or regulatory proteins may, through a similar mechanism, regulate the function of other ion channels or enzymes that contain VSDs. Introduction of charged residues at position 397 in the BK channel alters voltage-sensor activation, suggesting that interactions between the VSD and native charged residues in the cytosolic domain may normally exist and influence VSD function even in the absence of a charged ligand. A similar example may involve the cytosolic tetramerization (T1) domain of Kv channels where mutation of some charged residues facing the transmembrane domain produce large shifts in the voltage dependence of channel activation through unknown mechanisms (39, 40). Importantly, charges in the cytosolic domain of the BK channel do not act merely to bias the voltage detected by the VSD, as in the case of surface-charge effects (41). Rather, the impact of these charges varies as the relative position of cytosolic and VSDs change during channel opening. Similarly, it is possible that conformational changes in the cytosolic domain induced by neutral ligands or ligands distal from the VSD may expose the VSD to native charges to alter the activation of channels and enzymes. Finally, the VSD may be regulated by signaling processes other than ligand binding because posttranslational modifications such as phosphorylation, sulfation, oxidation, protonation, and methylation can increase or decrease the charge of amino acid side chains in cytosolic domains.

Methods

Mutagenesis and Expression. All channel constructs were made from the mbr5 clone of the mouse Slo1 BK (mSlo1) by using PCR with *Pfu* polymerase (Stratagene, La Jolla, CA). The PCR-amplified regions of all mutants were verified by sequencing. RNA was transcribed *in vitro* with T3 polymerase (Ambion, Austin, TX). We injected 0.05–50 ng (for macroscopic currents and limiting P_{open} recordings) or 150–250 ng (for gating currents) of RNA into each *Xenopus laevis* oocyte 2–6 days before recording.

Electrophysiology. Ionic currents were recorded with inside-out patches with an Axopatch 200-B patch-clamp amplifier (Axon Instruments, Union City, CA) and Pulse acquisition software (HEKA Electronik, Lambrecht/Pfalz, Germany) (19). The pipette solution contains 140 mM $KMeSO_3$, 20 mM Hepes, 2 mM KCl, and 2 mM $MgCl_2$, pH 7.2. The internal solution contains 140 mM $KMeSO_3$, 20 mM Hepes, 2 mM KCl, and 1 mM *N*-(2-hydroxyethyl)ethylenediamine-*N*,*N*′,*N*′-triacetic acid (HEDTA), pH 7.2. $CaCl_2$ was added to the internal solution to give the appropriate free intracellular Ca^{2+} concentration ($[Ca^{2+}]_i$), which was measured with a calcium-sensitive electrode. For 0 $[Ca^{2+}]_i$, the same internal solution was used except that HEDTA was substituted by 5 mM EGTA and no $CaCl_2$ was added. The basal internal solution for ionic strength experiments contains 20 mM Hepes, 15 mM KOH and 5 mM EGTA for 0 $[Ca^{2+}]_i$ and 20 mM Hepes, 6.5 mM KOH for 200 μM $[Ca^{2+}]_i$, pH 7.2. KCl was added to reach the target $[K^+]_i$s. A sewer pipe flow system was used to perfuse the internal solution on the cytosolic face of the patch. P_o (<0.01–0.1) at negative voltages was measured by single-channel recordings in patches containing hundreds of channels (17, 33).

Gating currents were recorded with inside-out patches (31). The pipette solution contains 127 mM tetraethylammonium hydroxide,

125 mM $HMeSO_3$, 2 mM HCl, 2 mM $MgCl_2$, and 20 mM Hepes, pH 7.2. The internal solution contains 141 mM *N*-methyl-D-glucamine, 135 mM $HMeSO_3$, 6 mM HCl, 20 mM Hepes, and 5 mM EGTA, pH 7.2. $MgCl_2$ was added to the internal solution to reach 10 mM $[Mg^{2+}]_i$. Voltage commands were filtered at 20 kHz with an eight-pole Bessel filter (Frequency Devices, Haverhill, MA) to prevent the saturation of fast capacitive transients (31). Data were sampled at 100,000 Hz with an 18-bit A/D converter (ITC-18; Instrutech, Mineola, NY) and filtered at 10 kHz with Axopatch's internal filter. Capacitive transients and leak currents were subtracted by using a P/5 protocol with a holding potential of −120 mV.

Chemical Modification. MTSET ([2-(trimethylammonium)ethyl] methanethiosulfonate bromide) and MTSEA (2-aminoethyl methanethiosulfonate hydrobromide) were purchased from Toronto Research Chemicals (Downsview, Canada). An aliquot of 100 mM MTS reagents stock solution was thawed and diluted 500-fold into the basal internal solution immediately before use. In ionic current recordings, currents were recorded after 2.5 min of MTS reagents treatment and 0.5 min of washing of patches with the inside-out configurations. In gating current recordings, MTSET was added directly into the bath.

Data Analysis. For macroscopic current, relative conductance was determined by measuring tail current amplitudes at −80 mV. The gating charge movements were determined by integrating the area under the rising phase and single exponential fits to the decaying phase of I_{gON} at various voltages. The conductance-voltage (G-V) relations or the charge-voltage (Q_c-V) relations of the WT and mutant channels were fitted with the Boltzmann equation:

$$G/G_{Max} = 1/(1 + \exp(-ze(V - V_{1/2})/kT)) \quad [4]$$

or

$$Q/Q_{Max} = 1/(1 + \exp(-z_J e(V - V_{hC})/kT)). \quad [5]$$

In Eq. **4**, z is the number of equivalent charges, $V_{1/2}$ is the voltage for channel in half-activation, e is the elementary charge, k is Boltzmann's constant, and T is the absolute temperature. In Eq. **5**, z_J is the gating charge associated with voltage sensor movement, V_{hc} is the voltage for half of the gating charge movements at the closed conformation of the channel, and the other parameters are as in Eq. **4**. The data were obtained from n = 4–16 patches. Error bars represent the SEM in all figures.

HCA Model Fitting. P_o-V relation at negative voltages, G-V and Q_c-V relations at 0 $[Ca^{2+}]_i$ were fitted to Eq. **6** derived from the HCA model (33),

$$P_o = 1\Big/\left(1 + \frac{1}{L_0}\left(\frac{1 + \exp(z_J F(V - V_{hc}))}{1 + \exp(z_J F(V - V_{ho}))}\right)^4 \exp(-z_L FV/RT)\right), \quad [6]$$

where V_{hc} and V_{ho} are the voltages for half of the gating charge movements at the closed and the open conformation, respectively; z_J is the gating charge associated with voltage sensor movement; L_0 is the intrinsic equilibrium constant for the activation gate, and z_L is the charge associated with channel opening.

Our results indicate that mutation Q397R shifts the Q_o-V relation via changing the local voltage sensed by R213. R213 is likely to be located in the crevice among the VSD, pore and cytosolic domains and exposed to the aqueous solution when interacting with R397, which is located at the border between a low dielectric (protein of the cytosolic domain) and a high dielectric (water in the crevice) medium. Thus, the distance between the charges of R213 and R397, r = 9.1 Å, can be calculated from the following equation (42, 43):

$$\psi_R = 2e\,\frac{\exp(-\kappa r)}{4\pi\varepsilon_0\varepsilon_r r}, \quad [7]$$

where $\Psi_R = 0.58^*\Delta V_{1/2}$, $\Delta V_{1/2}$ is the the Qo-V shift (−24 mV; Fig. 3 *f* and *g*), e is the elementary charge, ε_r is the dielectric constant of water, ε_0 is the permittivity of free space, and $1/\kappa$ (8.07 Å) is the Debye length in the aqueous phase and is calculated as in ref. 26.

Structural Model. The structure of Mg^{2+} binding site of the mSlo1 channel was generated based on the crystal structure of the MthK channel by using the PyMol molecular graphics system (www.pymol.org).

We thank Carol Deutsch, Toshi Hoshi, Zhe Lu, Colin Nichols, and Yasushi Okamura for critical discussions; Akansha Saxena for calculations of structural models; and Larry Salkoff (Washington University) for the mSlo1 clone. This work was supported by grants from the National Institutes of Health (F.T.H. and J.C.). J.C. is Associate Professor of Biomedical Engineering on the Spencer T. Olin Endowment.

1. Long SB, Campbell EB, Mackinnon R (2005) *Science* 309:897–903.
2. Murata Y, Iwasaki H, Sasaki M, Inaba K, Okamura Y (2005) *Nature* 435:1239–1243.
3. Ramsey IS, Moran MM, Chong JA, Clapham DE (2006) *Nature* 440:1213–1216.
4. Sasaki M, Takagi M, Okamura Y (2006) *Science* 312:589–592.
5. Hille B (2001) *Ion Channels of Excitable Membranes* (Sinauer, Sunderland, MA).
6. Perozo E, Bezanilla F (1990) *Neuron* 5:685–690.
7. Jones LP, Patil PG, Snutch TP, Yue DT (1997) *J Physiol (London)* 498:601–610.
8. Bao L, Cox DH (2005) *J Gen Physiol* 126:393–412.
9. Orio P, Latorre R (2005) *J Gen Physiol* 125:395–411.
10. Terlau H, Heinemann SH, Stuhmer W, Pongs O, Ludwig J (1997) *J Physiol (London)* 502:537–543.
11. Magleby KL (2003) *J Gen Physiol* 121:81–96.
12. Salkoff L, Butler A, Ferreira G, Santi C, Wei A (2006) *Nat Rev Neurosci* 7:921–931.
13. Ledoux J, Werner ME, Brayden JE, Nelson MT (2006) *Physiology (Bethesda)* 21:69–78.
14. Diaz L, Meera P, Amigo J, Stefani E, Alvarez O, Toro L, Latorre R (1998) *J Biol Chem* 273:32430–32436.
15. Ma Z, Lou XJ, Horrigan FT (2006) *J Gen Physiol* 127:309–328.
16. Stefani E, Ottolia M, Noceti F, Olcese R, Wallner M, Latorre R, Toro L (1997) *Proc Natl Acad Sci USA* 94:5427–5431.
17. Cui J, Aldrich RW (2000) *Biochemistry* 39:15612–15619.
18. Hu L, Shi J, Ma Z, Krishnamoorthy G, Sieling F, Zhang G, Horrigan FT, Cui J (2003) *Proc Natl Acad Sci USA* 100:10488–10493.
19. Shi J, Krishnamoorthy G, Yang Y, Hu L, Chaturvedi N, Harilal D, Qin J, Cui J (2002) *Nature* 418:876–880.
20. Xia XM, Zeng X, Lingle CJ (2002) *Nature* 418:880–884.
21. Yang H, Hu L, Shi J, Cui J (2006) *Biophys J* 91:2892–2900.
22. Jiang Y, Lee A, Chen J, Cadene M, Chait BT, MacKinnon R (2002) *Nature* 417:515–522.
23. Jiang Y, Pico A, Cadene M, Chait BT, MacKinnon R (2001) *Neuron* 29:593–601.
24. Fodor AA, Aldrich RW (2006) *J Gen Physiol* 127:755–766.
25. Kim HJ, Lim HH, Rho SH, Eom SH, Park CS (2006) *J Biol Chem* 281:38573–38581.
26. Elinder F, Arhem P (1999) *Biophys J* 77:1358–1362.
27. Zeng XH, Xia XM, Lingle CJ (2005) *J Gen Physiol* 125:273–286.
28. Hu L, Yang H, Shi J, Cui J (2006) *J Gen Physiol* 127:35–50.
29. Zhang X, Solaro CR, Lingle CJ (2001) *J Gen Physiol* 118:607–636.
30. Zhang G, Horrigan FT (2005) *J Gen Physiol* 125:213–236.
31. Horrigan FT, Aldrich RW (1999) *J Gen Physiol* 114:305–336.
32. Horrigan FT, Aldrich RW (2002) *J Gen Physiol* 120:267–305.
33. Horrigan FT, Cui J, Aldrich RW (1999) *J Gen Physiol* 114:277–304.
34. Krishnamoorthy G, Shi J, Sept D, Cui J (2005) *J Gen Physiol* 126:227–241.
35. Wallner M, Meera P, Toro L (1996) *Proc Natl Acad Sci USA* 93:14922–14927.
36. Shi J, Cui J (2001) *J Gen Physiol* 118:589–606.
37. Ye S, Li Y, Chen L, Jiang Y (2006) *Cell* 126:1161–1173.
38. Pathak M, Kurtz L, Tombola F, Isacoff E (2005) *J Gen Physiol* 125:57–69.
39. Robinson JM, Deutsch C (2005) *Neuron* 45:223–232.
40. Minor DL, Lin YF, Mobley BC, Avelar A, Jan YN, Jan LY, Berger JM (2000) *Cell* 102:657–670.
41. MacKinnon R, Latorre R, Miller C (1989) *Biochemistry* 28:8092–8099.
42. McLaughlin S (1989) *Annu Rev Biophys Biophys Chem* 18:113–136.
43. Elinder F, Mannikko R, Larsson HP (2001) *J Gen Physiol* 118:1–10.